SLOVAK UNIVERSITY OF TECHNOLOGY IN BRATISLAVA
Faculty of Electrical Engineering and Information Technology

Reg. No.: FEI-104354-70029

Ing. Hoang Vu Viet

Dissertaion Thesis Abstract

Development of a methodology and platform for the measurement of low-frequency magnetic field biological effects

to obtain the Academic Title of „Philosophiae Doctor“, abbreviated as „PhD.“

Study Programme:	Measurement Technology
Field of Study:	Electrical and Electronics Engineering
Form of Study:	Full-time

Bratislava 2025

Dissertation Thesis has been prepared at:
Institute of Measurement Science, Slovak Academy of Sciences

Submitter: Ing. Hoang Vu Viet
Institute of Measurement Science
Slovak Academy of Sciences
Dúbravská cesta 9
841 04 Bratislava 4, Slovakia

Supervisor: Mgr. Michal Teplan, PhD.
Institute of Measurement Science
Slovak Academy of Sciences
Dúbravská cesta 9
841 04 Bratislava 4, Slovakia

Consultant: Ing. Lubomír Kremnický, PhD.
Institute of Chemistry
Slovak Academy of Sciences
Dúbravská cesta 9
841 04 Bratislava 4, Slovakia

Reviewers: prof. Ing. Ladislav Janoušek, PhD.
Faculty of Electrical Engineering and Information Technology
University of Žilina
Univerzitná 8215/1
010 26 Žilina, Slovakia

doc. RNDr. Martin Kopáni, PhD.
Faculty of Medicine
Comenius University in Bratislava
Špitálska 24
813 72 Bratislava, Slovakia

Dissertation Thesis Abstract was submitted: ....

Dissertation Thesis Defence will be held on .... at ....
at the Faculty of Electrical Engineering and Information, Slovak University of Technology in Bratislava, Ilkovičova 2961, 841 04 Karlova Ves, Slovakia

....	....
prof. Ing. Vladimír Kutiš, PhD	doc. RNDr. Viktor Witkovský, CSc.
Dean of FEI STU	Director of IMS SAS

Abstract

Weak low-frequency magnetic fields (LF MF; 50-60 Hz) are widespread, yet their biological relevance remains uncertain due to inconsistent methods and environmental variability in prior studies. This dissertation addresses that gap by proposing and validating a rigorously controlled exposure platform for assessing LF MF effects on living cells, demonstrated with *Saccharomyces cerevisiae* as a model. The approach combines a pair of thermally stabilized cultivation chambers with homogeneous coil exposure and two complementary measurements of growth: a robust reference calibrated optical turbidimetry and electrical impedance spectroscopy. Using this framework, we evaluate whether LF MF alters yeast growth under well-defined conditions. Methodologically, we show that multiple interacting factors confound impedance-based cell concentration estimation, whereas turbidimetry provides reliable quantification. Biologically, across replicated temperature-symmetric experiments, no significant LF MF effect on yeast growth is detected. The contribution is a transparent, reproducible framework hardware, controls, and analysis that clarifies measurement limits and offers a foundation for future studies and biotechnological applications, including potential diagnostic or therapeutic uses based on electromagnetic inhibition or stimulation.

Keywords: low-frequency magnetic fields; Saccharomyces cerevisiae; real-time monitoring; impedance spectroscopy; turbidimetry; cell concentration estimation.

List of Symbols

Symbol	Unit	Description
B	H	Magnetic Flux Density
C	F	Capacitance
C_m	F	Membrane Capacitance
ΔC	F	Capacitance Increment
E_2	-	Biomass Estimator
f	Hz	Frequency
f_c	Hz	Characteristic Frequency
N, N_c	-	Cell Concentration
r	m	Radius of the Shell-sphere
t	s	Time
T	°C	Temperature
ΔT	°C	Difference in Temperature
Z	Ω	Impedance
$Im(Z)$	Ω	Imaginary Part of Impedance
$Re(Z)$	Ω	Real Part of Impedance
ε	F/m	Relative Permittivity
ε_0	$8.85\ 10^{-12}$ F/m	Permittivity of Vacuum
$\Delta\varepsilon$	F/m	Permittivity Difference
κ	S/m	Relative Conductivity
ε_a, κ_a	F/m, S/m	Relative Permittivity and Conductivity of the Medium
σ_e	S/m	Extracellular Conductivity
σ_i	S/m	Intracellular Conductivity
ϕ	Wb	Magnetic Flux

List of Abbreviations

C	Control
C/C	Control/Control
CCY	The Culture Collection of Yeasts
EIS	Electrical Impedance Spectroscopy
EMF(s)	Electromagnetic Field(s)
EU	European Union
DNA	Deoxyribonucleic acid
DCR	Direct Current Resistance
HF	High Frequency or High-frequency
ICNIRP	International Commission on Non-Ionizing Radiation Protection
IS	Impedance Spectroscopy
LCB	Low conductivity buffer
LF	Low Frequency or Low-frequency
Log	Logarithmic
MF(s)	Magnetic Field(s)
NTU	Nephelometric Turbidity Units
PBMC	Peripheral Blood Mononuclear Cell
PCR	Polymerase Chain Reaction
PD	Photodiodes
PI	Propidium Iodide
PID	Proportional-Integral-Derivative
PMT	Photomultiplier Tubes
ROS	Reactive Oxygen Species
RPM	Revolution per minute
RSD	Relative Standard Deviation
SAL	Sterility Assurance Level
SD	Standard Deviation
T	Test
T/T	Test/Test
TTF(s)	Tumour Treating Field(s)
UV	Ultraviolet
YPD	Yeast Extract Peptone Dextrose

Table of Contents

1 Introduction

Low-frequency magnetic fields (LF MFs), typically Hz–kHz, are ubiquitous from power lines, appliances, and industrial systems. Interest centers on network frequencies (50/60 Hz), yet despite many reports of bioeffects, mechanisms and implications for health and biotechnology remain unclear due to heterogeneous methods and contexts.

In residential and office environments across the European Union (EU), typical 50 Hz magnetic flux densities are in the range of about 0.01-0.2 µT, with median values around 0.03-0.04 µT in most dwellings [1], [2], [3]. Regulatory guidelines emphasize that these values are orders of magnitude below international safety thresholds; for example, the International Commission on Non-Ionizing Radiation Protection (ICNIRP) 2010 sets a reference level of 200 µT at 50 Hz, while the EU recommends 100 µT as the reference level for general public exposure [4], [5].

A substantial literature reports both beneficial and detrimental LF MF outcomes across cellular processes (ion channels, cytoskeleton, gene expression, signaling, ROS), with effects on proliferation and oxidative stress and suggested links to cancer and cardiovascular disease [6]–[16]. Therapeutic explorations (e.g., regeneration, wound healing, oncology, neuroprotection) and biotechnological applications in microbes and plants have also been proposed, but results remain mixed and often context-dependent [17]–[21],[22], [23]. These inconsistencies underscore the need for systematic, well-controlled studies.

At cellular and physiological levels, responses vary by model and conditions: reports range from inhibited or enhanced growth (including in S. cerevisiae) to protective effects against cell death, while some studies suggest nervous-system sensitivity though findings are inconsistent [8], [9], [13], [19], [21], [24]. Several physical interaction hypotheses ion cyclotron/parametric resonance and radical-pair mechanisms have been proposed, yet rigorous experimental support is limited, partly due to sparse frequency sampling; "window" effects remain an open question [25]–[33].

Methodological limitations persist inconsistent exposure setups, inadequate temperature control, insufficient shielding from magnetic noise, and incompletely characterized systems hinder reproducibility and credibility [34], [35]. The 2020 ICNIRP report and subsequent analyses call for standardized, rigorous frameworks to resolve these issues [36]–[38]. Motivated by these insights and by insufficient thermal control in many

50/60 Hz studies [7]–[9], [13], [19], [24], [39] this thesis develops a robust platform emphasizing precise environmental control and standardized biological assessment.

Here, we present and validate a platform that generates well-defined LF MFs and supports real-time biological monitoring. It prioritizes temperature stability, field homogeneity, parallel test–control configurations, and reproducible cultivation. Using S. cerevisiae as a model, we evaluate LF MF effects on growth with improved accuracy, reproducibility, and interpretability, aiming to reduce uncertainty in the field and enable well-controlled applications in basic science and biotechnology.

Aims of the dissertation thesis

To sum up the focus of the dissertation thesis, our main objectives are as follows:

1. Gathering knowledge about the state of the art in experimental evidence, theoretical models, as well as methods for measurement of biological response of living cells to low-frequency magnetic fields.

2. Development of experimental platform allowing characterization of biological effects of LF MF on living cells. Modification of available module components and their mutual compatibility.

3. Selection of a cell concentration estimation method that is feasible on the developed experimental platform.

4. Realization of real-time monitoring of cell concentration based on impedance spectroscopy.

5. Development of a new measurement methodology based on electric impedance spectroscopy for assessment of the effects of LF MF on living cells.

6. Expansion of the knowledge about the influence of external LF MF on selected biological objects, potentially applicable in biotechnology and medicine.

2 Biological Effects and Mechanisms of Interaction

Research into the biological effects of LF MFs has steadily grown over the past decades, driven by their widespread presence in modern life and the persistent uncertainties surrounding their physiological influence. Numerous studies have investigated their effects on various organ systems and cell types, yielding both promising results and significant contradictions. This chapter reviews key findings in the literature, ranging from systemic physiological responses such as impacts on the immune, reproductive, and nervous systems to cellular-level experiments examining proliferation. In doing so, it also highlights major methodological challenges in the field and the need for improved experimental control, which this thesis aims to address.

LF MFs have been reported to modulate immune, reproductive, cardiovascular, nervous, and metabolic functions, but outcomes are dose-, time-, and model-dependent. Low–moderate exposures can alter immune markers and cytokines, while higher intensities may suppress lymphocyte activity; reproductive findings range from hormone shifts to null effects; cardiovascular studies show mixed results from transient heart rate or calcium changes to no long-term alterations; and neural studies report both neuroprotective signals and inconsistent functional changes. Some work hints at therapeutic potential (e.g., microcirculation, autonomic modulation), yet conflicting evidence and variable methods limit inference. Overall, the balance of findings underscores the need for rigorously controlled, temperature-symmetric, and well-characterized exposure designs [40].

Proposed mechanisms include weak induced electric fields and currents (membrane polarization), modulation of voltage-gated ion channels, and spin-chemistry effects on radical pairs that can shift reactive oxygen species (ROS). Among these, radical-pair–mediated ROS modulation currently offers the most cohesive, non-thermal explanation across systems, whereas resonance-based ion models remain intriguing but sparsely validated. Induced transmembrane effects are typically small yet could matter in highly sensitive contexts. The experimental platform developed here emphasizing field homogeneity, real-time readouts, and strict environmental control is designed to test these hypotheses under biologically relevant, reproducible conditions [41]–[44].

2.1 Research Overview of LF MF Effects

The influence of LF MFs on biological systems remains an active area of research with both promising applications and unresolved controversies. Numerous vitro studies have explored how magnetic field parameters such as frequency, flux density, and exposure duration affect various cellular outcomes [45].

Tab. 1 summarizes nine representative studies investigating the impact of LF MF exposure on different cell types, ranging from *Saccharomyces cerevisiae* to human dermal fibroblasts, microglial cells, and several cancer and stem cell lines. The experimental protocols and outcomes vary widely, with reported results including enhanced proliferation, apoptosis induction, DNA synthesis disruption, or complete absence of measurable effects. This variability underscores the complexity of LF MF interactions with cellular systems and highlights the importance of methodological rigor in the design of exposure experiments.

Notably, some studies report frequency or magnetic flux density dependent effects. Zhang et al. (2013) [8] observed enhanced proliferation in human epidermal stem cells at 50 Hz, while Radil et al. (2020) [46] reported frequency-dependent inhibition of *Saccharomyces cerevisiae* proliferation in the range of 0.4–1.6 kHz. Meanwhile, Song et al. (2018) [39] found that a 60 Hz, 6 mT field promoted proliferation in HeLa and fibroblast cells, attributing this to reduced reactive oxygen species. Conversely, Xu et al. (2020) [19] demonstrated that similar LF MF exposure triggered apoptosis in breast cancer cells while sparing non-cancerous lines. These opposing results raise the question of cell type specificity, exposure parameter tuning, and whether some cellular systems are more prone to LF MF influence than others.

Tab. 1: Summary of experimental parameters and biological responses to LF MF exposure. This table compares LF MF exposure conditions across selected studies, including magnetic field frequency and intensity, exposure duration, biological models, temperature settings, measurement methods, and observed cellular responses. Results show a wide variability in both experimental design and biological outcomes, underscoring the complexity of LF MF interactions and the need for standardized protocols.

Reference	MF		Exposure duration	Biological Model	T [°C]	Measurement Method	Result
	Frequency [Hz]	Flux density [mT]					
Novak, 2006	60	10	60min	S. cerevisiae	24-26	optical density	inhibiting effects
Zhang, 2013	50	5	7days, 30m/day	hESC	37	flow cytometry	cells increased during the S phase
Lee, 20015	60	0.01~1	4h~16h	MCF10A,NIH3T3	20-30	hemocytometer	decreased viability, DNA synthesis
An, 2015	50	2.3	2h/d,5d/w	KYSE150, C6	37	hemocytometer	no change in cell morphology
Pasi, 2016	5&50	0.25~1.6	1.5h	fibroblasts	37	hemocytometer	no changes in cell viability
Duong, 2016	10/50/100	0.01~1	4h	HMO6	37	hemocytometer	cell death detected
Song, 2018	60	6	1h/d, 3d	HaCaT, PC12, NIH-3T3	37	flow cytometry	promoted cell proliferation
Xu, 2020	50-275	1	6h~36h	MCF-7, ZR-75-1, T47D	n/a	flow cytometry	inhibiting effects via apoptosis
Radil, 2020	0.4~1.6k	2.33~2.45	72h	S. cerevisiae	27	Petri- Counter	inhibiting effects

2.2 Lack of Control and Reproducibility in LF MF Research

A deeper review of study designs (Tab. 2) shows major inconsistencies in managing environmental and exposure conditions. Temperature control is the most frequent gap: only a few studies (e.g., Lee 2015 [7], Pasi 2016 [9], Radil [46], An 2015 [47]) reported temperature, and even then, without full profiles for both control and test groups. Most assumed incubator stability or used coarse settings, despite the strong temperature sensitivity of cellular processes small drifts can be misread as LF MF effects.

Exposure symmetry is also underused. Beyond test–control comparisons, rigorous designs should include control/control (C/C) and test/test (T/T) replications and, ideally, cross-over (swapping exposure between groups) to reveal spatial biases or coil asymmetries. Few studies added these elements, and none used a full cross-over design. Likewise, ΔT (T–C) the temperature difference between test and control was rarely tracked, obscuring separation of thermal from non-thermal effects, especially in long culture runs. Together, weak thermal control, limited internal validation, and absent cross-over testing point to a need for stricter, more transparent protocols.

In summary, intriguing LF MF findings are undermined by methodological heterogeneity. Field-wide standardization, especially continuous temperature monitoring, exposure symmetry, and stronger control design with real-time readouts are essential for definitive conclusions.

Our response is a modular, tightly controlled platform: precise temperature regulation with active feedback and dual-sensor monitoring on both test and control; environmental stability within and across compartments to minimize differential heating and interference; and parallel, swappable exposure channels that enable C/C, T/T, and full cross-over (T/C ↔ C/T) experiments. This architecture reduces systematic bias and supports reproducible studies that clarify LF MF biological relevance and inform future therapeutic/biotechnological applications.

Tab. 2: Evaluation of experimental design quality and environmental control in LF MF studies. This table analyses methodological rigor in selected LF MF experiments based on criteria such as repetition, use of pair controls, temperature monitoring, and experimental symmetry. Key factors like ΔT (temperature difference between test and control), C/C and T/T pair experiment, and cross-over design are largely missing, indicating common limitations in reproducibility and environmental consistency.

Reference	Repetition Number	Pair Experiment	Climated Room	Temperature Monitoring	ΔT reported (T-C)	C/C; T/T tests	Cross-over design
Novak, 2006	10, 4	Yes, 2 different places, 1 coil	No	No, room temperature	No	No	No
Zhang, 2013	3-4	Yes, 2 incubators	No	Incubator set to 37.0 °C ± 0.5; no further monitoring	No	No	No
Lee, 20015	>=3	Yes	No	Yes; both T and C monitored and maintained at 37 ± 3 °C	No	No	No
An, 2015	>=3	Yes, 1 incubator	No	Incubator's temperature is monitored, but not temperature of both samples	No	No	No
Pasi, 2016	3	Yes, 2 different places, 1 coil	No	Yes; temperature stability kept within 1 °C; no further details	No	No	No
Duong, 2016	9.12	Yes, 1 incubator	No	No	No	No	No
Song, 2018	3	Yes, 1 coil	No	No	No	No	No
Xu, 2020	>=3	Yes, 2 incubator	No	No	No	No	No
Radil, 2020	>=3	Yes, 2 incubators, 2 coils	No	Yes; both incubators kept at 27 °C, confirmed by thermometer	No	No	No

3 Cell Concentration Estimation Methods

Accurate estimation of cell concentration and viability is essential across microbiological research, yet cell counting is prone to numerous pitfalls. To mitigate these issues, recent decades have seen significant advances that make counting increasingly reliable and highly automated.

3.1 Hemocytometer

Despite many automated options, the hemocytometer remains a practical “gold standard” for cell counting across diverse samples (blood, cultures, urine, water), often with a viability dye such as Trypan Blue to distinguish live/dead cells. It is a glass slide with a 9 square grid (each large square 1 mm × 1 mm, subdivided to 0.00025 mm^2) and, under a coverslip, a chamber height of 0.1 mm so the counted volume is precisely defined. Typical practice is to count cells (4×–10× objective) in the four corner squares, average them, and compute concentration as the average × 10^4 × dilution factor. For reliable statistics, aim for ~100–200 cells per 1 mm^2; dilute or concentrate accordingly. Accuracy is limited by mixing, pipetting, and operator differences, so replicate independent counts are recommended to reduce variability.

3.2 Turbidimetry

Turbidimetry estimates cell concentration by measuring how suspended particles reduce transmitted light through a sample: monochromatic light passes a cuvette, a detector records the transmitted beam, and the drop in intensity reflects scattering and absorption by the cells. Because cell scattering is elastic, scattered and incident wavelengths match; the instrument effectively quantifies forward transmission (conceptually like absorption spectrophotometry) to infer particle abundance. Results are often expressed in Nephelometric Turbidity Units (NTU), which scale with the amount of light scattered and thus with biomass density providing a rapid, non-invasive way to track microbial growth over time (e.g., yeast cultures).

3.3 Electrical Impedance

Electrical impedance spectroscopy (EIS) provides a non-invasive, real-time readout for suspensions in conductive media, interpreted through simplified physical models that relate measured spectra to cellular properties.

Cell membranes behave capacitively, making impedance strongly frequency dependent: low frequencies yield higher impedance and larger phase angles, while membrane reactance diminishes as frequency increases. The complex permittivity shows distinct dielectric dispersions; for biomass estimation the most informative is the β-dispersion (~100 kHz–10 MHz) dominated by membrane polarization at the cell–medium interface. Lower α-dispersion (<1 kHz) largely reflects electrode polarization and interfacial effects, whereas the γ-dispersion (GHz) is governed by water. Our analysis targets the β region where concentration-dependent changes are most reliably captured for non-invasive monitoring.

Approach I

One approach to estimating cell concentration from impedance data relies on analyzing the dielectric dispersion characteristics of cell suspensions, as proposed by K. Asami and T. Yonezawa. This method interprets the frequency-dependent dielectric response of the medium to derive biologically relevant parameters. Their studies demonstrated that dielectric spectroscopy could serve as a reliable technique for tracking cell concentration over time. [48].

Using the single-shell (Pauly–Schwan–type) model cells as conducting spheres with thin capacitive membranes suspended in a conductive medium the β-dispersion amplitude of the suspension permittivity ($\Delta\varepsilon$) scales linearly with viable cell volume fraction and thus with cell concentration [51]. Under the usual dilute-suspension and thin-membrane assumptions, the resulting practical estimator is:

$$N_c = \frac{\varepsilon_0}{3\pi r^4 C_m}\Delta\varepsilon \tag{3.1}$$

where N_c is cell concentration, r the cell radius, C_m the membrane capacitance per area, and ε_0 the vacuum permittivity.

Approach II

Another method to estimate cell concentration from impedance data was developed by Yardley et al. [49], and it shares a conceptual similarity with the dielectric dispersion-based approach of K. Asami and T. Yonezawa. Both methods rely on the characteristic dielectric behavior of cell suspensions in response to an applied alternating electric field. However, while Asami's model analyzes the entire frequency-dependent curve and extracts parameters using a physical model of spherical shell particles, Yardley's approach simplifies the estimation by focusing on a specific dielectric feature across two frequencies.

The method focuses on the capacitance increment (ΔC), defined as the difference between the measured capacitance at a low frequency, where intact cell membranes become polarized and the residual capacitance at a high frequency, where membrane polarization is negligible due to the field penetrating into the cell interior. This difference captures the membrane's contribution to the overall dielectric response.

From two selected frequencies $f_1<f_2$ within the β-dispersion derive the relative-permittivity change $\Delta\varepsilon$ (t, f_1, f_2), from the computed capacitance difference ΔC (via the electrode geometry factor). The estimated cell concentration is then:

$$N(t, f_1, f_2) = \frac{\varepsilon_0 \cdot 10^{-6}}{3\pi r^4 C_m} \cdot \Delta\varepsilon(t, f_1, f_2) \tag{3.2}$$

Where r = $2{\cdot}10^{-6}$ m is the assuming cell radius, C_m =$1.1{\cdot}10^{-2}$ F/m^2 is the specific assuming membrane capacitance of viable cells.

Approach III

Another approach introduced by Soley et al. [50], utilizes impedance spectroscopy to monitor yeast cell growth by analyzing the ratio between low-frequency and high-frequency impedance values. Instead of relying on capacitance increments like previous methods, this approach focuses on how the impedance spectrum evolves as biomass increases. The frequency-dependent shift in impedance is then used as a parameter to estimate cell concentration in real time. The estimator is calculated as following:

$$E_2 = 100\left(1 - \frac{|Z(HF)|}{|Z(LF)|}\right)(\%) \tag{3.3}$$

Where E_2 is the biomass estimator, $|Z(LF)|$ is the value of impedance magnitude at $f \ll f_c$ and $|Z(HF)|$ is the impedance magnitude at $f \gg f_c$.

The biomass estimator E_2 depends on cell radius r, membrane capacitance C_m, the volume fraction P, and the intra and extracellular conductivities σ_i and σ_e. Under the assumptions that $P < 0.2$ (v/v) and $\sigma_i \approx \sigma_e$, E_2 becomes linearly proportional to P and essentially independent of the other parameters [52]. In practice, for a given microorganism R, C_m, and σ_i are approximately constant, whereas σ_e may vary with medium composition and temperature.

4 Development of Experimental Platform

Design and development of an experimental platform is the first and most vital step of our research. Measuring instruments of the platform must be chosen appropriately in order to be compatible with each other while maintaining their required functionality. From the constructed foundation and experimental workflow of the platform, many modifications and improvements have been and are being applied.

4.1 The Experimental Workflow

Experiments use paired cultivation chambers run in parallel under nearly identical conditions, flexibly configured as test–control, test–test, or control–control to enable differential exposure and internal validation, minimizing variability and improving statistical power. As outlined in Fig. 1, a yeast strain from the CCY collection (SAS, Slovakia) maintained on solid medium serves as inoculum for pre-cultivation; the culture is then diluted, aliquoted into vials, and placed in chambers with active temperature regulation and independent monitoring to maintain tight thermal symmetry. The integrated magnetic system allows each channel to be set to exposure or control independently for precise LF MF application. After cultivation, cell concentration is measured, and data undergo structured filtering and verification; only validated datasets proceed to final statistical evaluation.

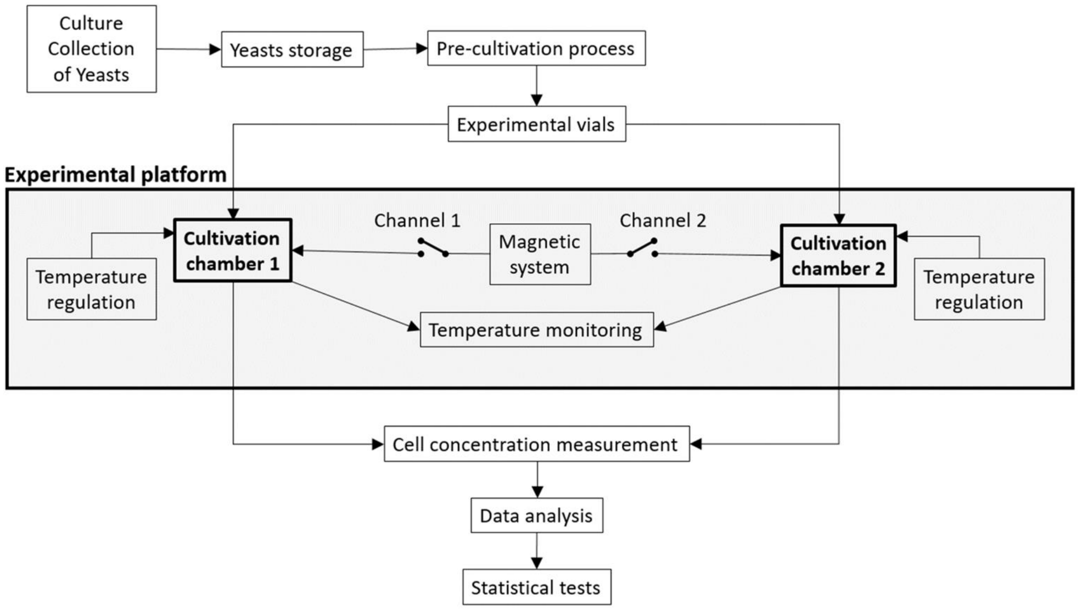

Fig. 1: Schematic diagram of the experimental workflow for low-frequency magnetic field exposure studies. The platform integrates two temperature-controlled cultivation chambers connected to a dual channel magnetic field generation system, implemented with temperature monitoring ensures thermal consistency.

4.2 Helmholtz Coils

To ensure uniform exposure over planar cell cultures, we targeted high homogeneity in the sample plane using a Helmholtz configuration. We modeled multilayer air-core coils across the Hz–kHz range under three constraints amplifier current limit, amplifier voltage/impedance, and a coil self-heating cap of 2 W and optimized coil geometry (turns, layers, wire gauge) to maximize center B while preserving lateral uniformity. The model shows a non-monotonic dependence of achievable field on turn count: added turns raise inductance and resistance, lowering current at a fixed drive and eventually reducing B. This guided selection of a geometry that balances field strength, homogeneity, and thermal safety, and satisfies the Helmholtz spacing criterion (coil separation ≈ radius).

We realized two identical air-core circular coils in Helmholtz layout: 50 turns of 2.2 mm Cu arranged in 5 layers × 10 turns, wound on 3D-printed spools (inner *Ø* = 116 mm, outer *Ø* =126 mm, avg. *Ø* ≈ 121 mm), mounted face-to-face with 60 mm separation to meet the Helmholtz condition. Electrical characterization gave DCR ≈ 0.185 Ω and 0.197 Ω (4-wire), and inductance per coil near 1 mH across 50 Hz–100 kHz with small coil-to-coil differences (typically < 3%) and expected high-frequency roll-off from parasitic capacitance. Field mapping confirms a flat central region and good lateral homogeneity over the culture area, matching simulations and supporting reproducible LF MF exposure.

4.3 System for Magnetic Field Generation

The magnetic exposure system comprises a Helmholtz coil pair driven by an Owon XDG3102 waveform generator and a Behringer NX3000D power amplifier, delivering up to 8 A (rms) from 0–2 kHz to generate fields up to 5 mT. It supports two operating modes: Bridge Mode, which combines both generator channels into one high-power output to drive a single coil (with a series potentiometer for load matching and oscilloscope monitoring for waveform integrity), and Dual Mode, which drives two coils independently each with a series variable resistor and ammeter for parallel, symmetric exposures in separate cultivation chambers. Field matching in paired experiments is high: at 800 Hz ($X_L \approx 5.03$ Ω), the flux-density ratio between chambers was ~1.01 (difference < 2%), confirming near-identical exposure conditions.

4.4 Homogeneity of Magnetic Field

To verify field homogeneity, we mapped magnetic flux density at 15 points inside a centrally placed 250 ml low-form beaker ($\varnothing$ = 76.5 mm), arranged in three horizontal planes (bottom, +6 mm, +12 mm) as shown in Fig. 2, positions were set with a SOMET INOX caliper (±0.01 mm), and axial B was read using a SYPRIS 7010 Gauss meter (AC accuracy ±1%; ±0.03 mT on the 3 mT range, ±0.3 mT on 30 mT). Sinusoidal drive (e.g., 3.5 Vpp at 1 kHz) was applied in bridge mode, with waveform and coil current monitored by oscilloscope and ammeter; results across conditions yielded relative standard deviations (RSD) of 1.64–2.57%, confirming high uniformity within the measured volume. No outliers or abrupt spatial drops were observed, with best uniformity near 1 kHz and slight deviations at higher/lower power. Because uniformity decreases away from the coil axis, the working volume was constrained (< 100 ml, centrally aligned) and, for non-stirred runs, sedimentation kept samples in the most homogeneous zone minimizing edge effects and ensuring reproducible exposure.

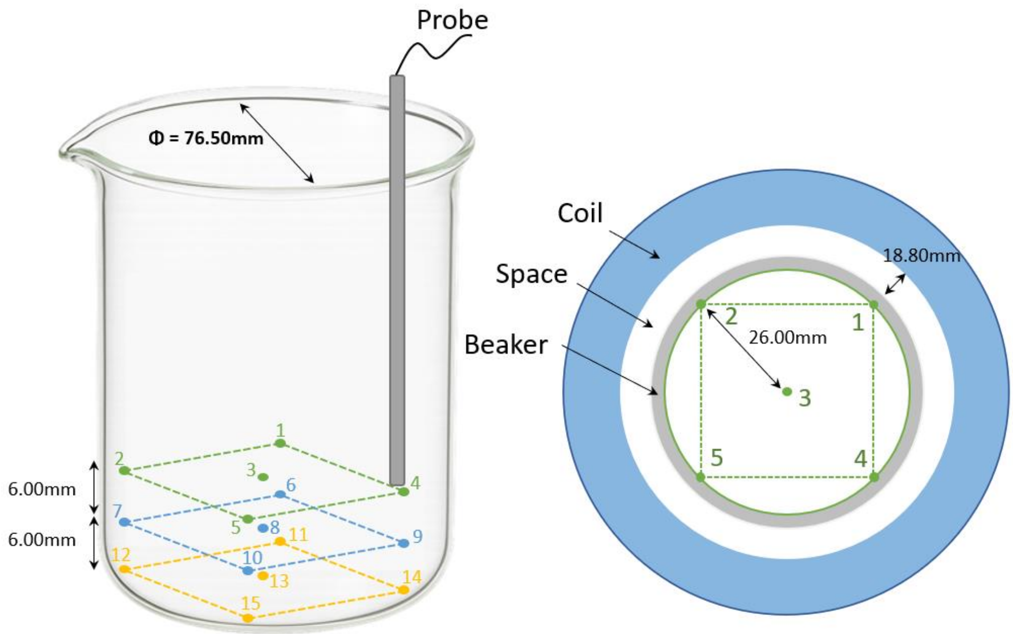

Fig. 2: Magnetic flux density of MF measuring locations inside the beaker.

4.5 Temperature Regulation in Cultivation Chamber

We first used an on–off controller in custom heated boxes (Candy CCV 150 EU) with foil heaters and K-type logging; after stabilization the sample temperature still oscillated ~30.7–33.7 °C (spread 3.0 °C; SD ≈ 0.54 °C), which was inadequate for yeast work (Fig. 3). We therefore implemented a PID regulator (Rex C100, Pt100 in the water bath) with auto-tuned gains (P = 1.8, I = 3600, D = 900) and Arduino monitoring (DS18B20, 10 s sampling), achieving long-term stability of ±0.3 °C (worst cases ≲ ±0.5 °C).

With the PID set to 35 °C, we mapped chamber temperatures using multiple sensors: one submerged in the water bath and two at different heights in air; even with the coils powered as an added heat source, the submerged probe held the set point (Fig. 4a, b). A 3D printed stand later fixed coil and vial geometry to improve airflow symmetry and thermal stability. Final placement used one submerged sensor per chamber for sample temperature and one ambient sensor (~1 m height) for room tracking.

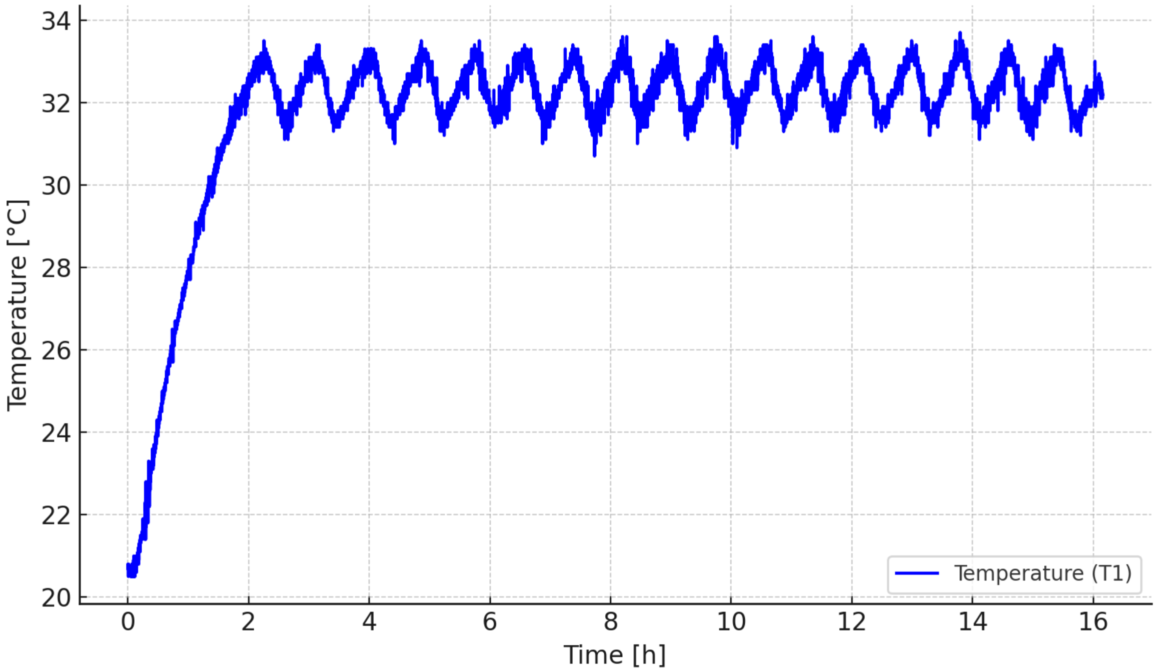

Fig. 3: Temperature profile recorded using an on-off temperature controller and K-type thermocouple sensor. After initial stabilization, the temperature oscillated between approximately 30.7 °C and 33.7 °C, resulting in a fluctuation of 3.0 °C.

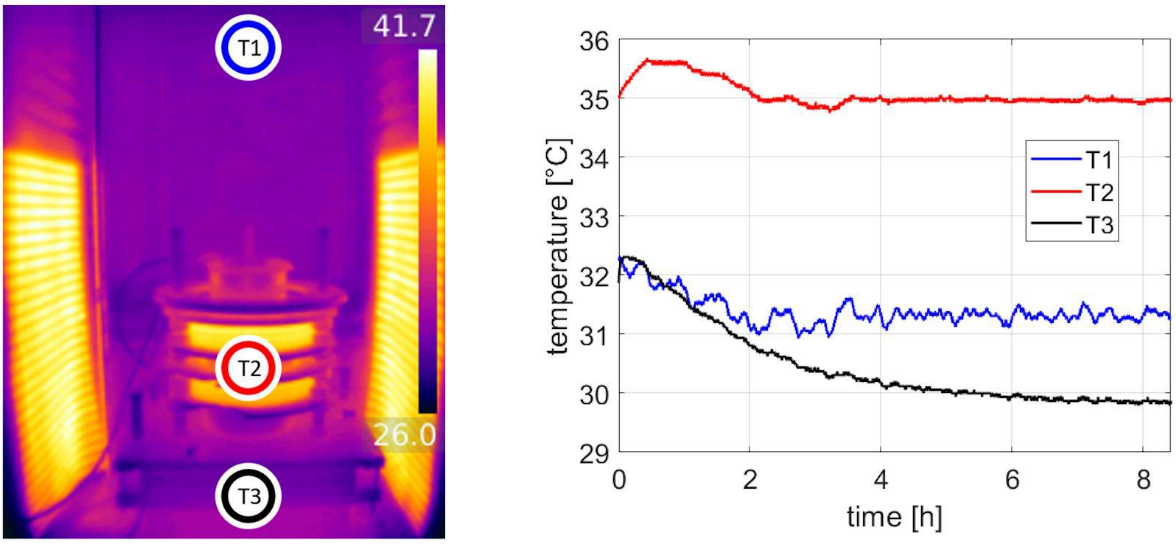

(a) (b)

Fig. 4: (a) thermal image of the Helmholtz coil system placed inside the cultivation chamber, (b) temperature stability test in the chamber with the PID controller set to 35 °C. T1 – top of the cultivation chamber, T2 – water bath in the beaker, T3 – bottom of the cultivation chamber.

4.6 In-situ Temperature Monitoring of Samples

A simple, robust temperature-logging system was built around an Arduino Uno with three DS18B20 digital sensors positioned to track Chamber 1, Chamber 2, and ambient air; wired on OneWire with pull-ups, it streamed timestamped readings over serial while displaying real-time values on an LCD. This replaced a K-type thermocouple logger whose dated software, awkward data format, and fragile leads hindered use. Data were saved to a text file and analyzed in a spreadsheet to compute means, standard deviations, and the chamber temperature difference ΔT; runs were accepted only when ΔT stayed within ±0.3 °C, ensuring tight thermal symmetry and minimizing confounds during weak low-frequency magnetic-field exposure experiments.

5 Cell Concentration Monitoring Based on Impedance Spectroscopy

We applied electrical impedance spectroscopy (EIS) for real-time estimation of yeast concentration using a wide-band, 4-wire analyzer (10 Hz–10 MHz) to acquire complex spectra with minimized electrode polarization. Three estimators were implemented: Approach I (Asami–Yonezawa, Eq. (3.1) mapping β-dispersion permittivity (from *Im(Z)*); Approach II using the capacitance increment (ΔC) between a low and a high frequency within β-dispersion Eq. (3.2); and Approach III impedance ratio, Eq. (3.3) comparing low- vs high-frequency $|Z|$. As shown in Fig. 5, Approaches I and II produced growth-like trajectories (including an exponential segment), whereas Approach III yielded decreasing curves under the chosen LF/HF pair, indicating a need for recalibration and/or sign handling.

Frequency choice was critical. For Approach I, a 300 kHz–4 MHz window provided stable, informative permittivity dynamics; much lower frequencies added noise, while much higher frequencies reduced dynamic resolution. Conductivity (κ) was taken from the real part of Z at low frequency to parameterize the model, with the characteristic frequency f_c incorporated via the standard factor in the final estimator. Fig. 6 demonstrates that differing measurement frequencies (20 kHz, 400 kHz, 3.2 MHz, 10 MHz) markedly shape the inferred concentration curves, and also that absolute permittivity offsets from probe wear shift the level but preserve curve shape, so Approach I, which relies on $\Delta\varepsilon$, is relatively robust to moderate electrode degradation. Reliable mid-range estimation therefore hinges on careful frequency selection, routine electrode maintenance, and frequency-specific calibration.

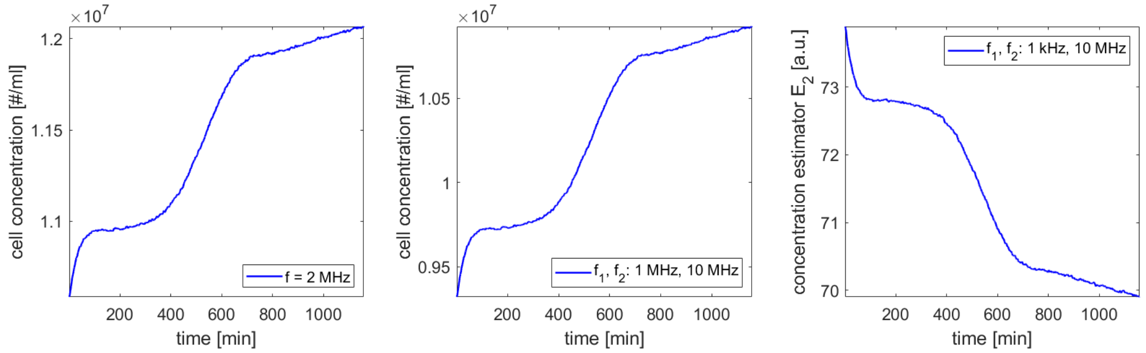

(a) (b) (c)

Fig. 5: Comparison of cell concentration estimation using three different impedance-based approaches. (a) Approach I based on dielectric dispersion modeling at a single frequency (2 MHz); (b) Approach II based on the capacitance increment (*ΔC*) between 1 MHz and 10 MHz; (c) Approach III based on the ratio of impedance magnitudes at 1 kHz and 10 MHz.

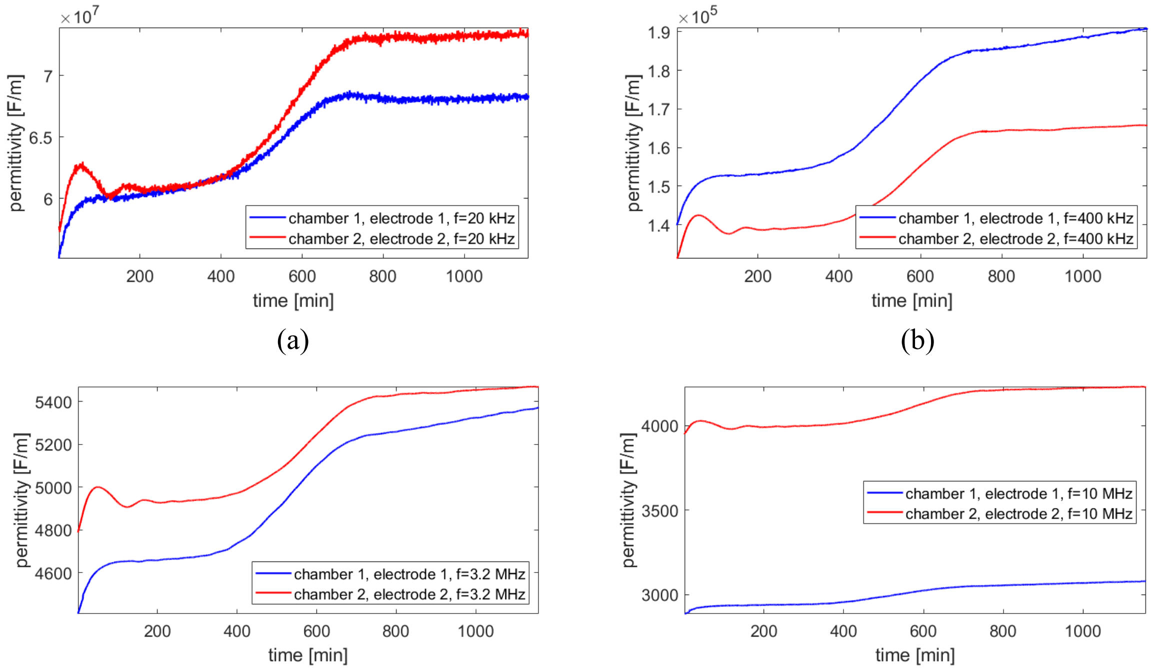

(a) (b) (c) (d)

Fig. 6: Example cell concentration curves calculated using the Asami and Yonezawa approach at different frequencies. (a) 20 kHz, (b) 400 kHz, (c) 3.2 MHz, and (d) 10 MHz. The two electrodes exhibited differing degrees of electrochemical degradation.

5.1 Methodology for Quantifying LF MF Effects from Impedance Spectroscopy Monitoring

To specifically quantify the effect of LF MF on cell growth, a novel, three-step analytical methodology was developed. This approach transforms raw impedance data from a pair experimental setup into a single, quantifiable metric of inhibition or stimulation.

Step 1: Calibration

The initial step focuses on making the two time-series curves of permittivity (Test conditions and Control conditions) comparable. Since the raw impedance-derived concentration curves (e.g., from Approach I at 3.2 MHz, as seen in Fig. 6c) appear visually unrelated, a two-point calibration is applied. This calibration anchors both the Test and Control curves using known initial and terminal cell concentrations. The initial concentrations, coming from the same prepared solution, are assumed to be identical. The terminal concentrations (after 18-20 h of cultivation) are determined by an independent method (turbidimetry or hemocytometer counts), typically showing minor differences. This procedure assumes a linear relationship between the calculated permittivity and cell concentration across the entire measured range.

Step 2: Normalization

The absolute concentration values are then transformed into the cell multiplication rate (Fig. 7, the blue and red curves referenced by the primary Y-axis). This rate measures the fold-increase of the cell population from the starting concentration. This transformation is preferred because the multiplication rate is more universal and easier to comprehend for comparing different experimental runs or setup conditions than the absolute cell concentration itself.

Step 3: Quantification via the Effect Ratio

To directly compare the two established cell multiplication rate curves and normalize the results, we define the Effect Ratio:

$$Effect\ Ratio\ (t) = \frac{Multiplication\ Rate_{Exposed}(t)}{Multiplication\ Rate_{Control}(t)} \tag{5.1}$$

The Effect Ratio provides a continuous, normalized measure of the field's influence over time, specifically quantifying the relative performance of the exposed sample compared to the control. In Fig. 7 it’s represented graphically by a black curve referenced by the secondary Y-axis.

Step 4: Single-Value Evaluation

The final step requires evaluating the entire experimental run with a single, quantitative value that reflects both the qualitative outcome (inhibition or stimulation) and its degree. Due to slight run-to-run variability in growth curve profiles - specifically, the magnitude of growth and the precise timing of the culmination point (maximum) after the exponential phase - fixing a single time point for final evaluation would be too restrictive. Instead, the evaluation time point was left to "float" within a reasonable short time window following the cessation of exponential growth. The single metric reflecting the maximum effect is determined naturally by the:

- Minimum value of the Effect Ratio curve (for the inhibition effect).
- Maximum value of the Effect Ratio curve (for the stimulation effect).

This procedure ensures the quantification captures the peak biological response regardless of minor shifts in the growth phase timing.

Methodological Validation and Preliminary Result of LF MF Effect

Fig. 7 presents a representative example of growth dynamics under LF MF exposure (3 mT at 800 Hz). A visible sign of inhibition in the exposed cell sample relative to the control appeared at approximately 600 min. The calculated Effect Ratio shown on the secondary Y-axis, reached its minimum value of 0.89 at approximately 750 min. This minimum quantitatively indicates that the concentration of the exposed sample was about 11% lower than that of the control sample at the point of maximum effect. It should be noted that the initial segment of the Effect Ratio curve exhibits a high level of noise, primarily due to the temperature stabilization phase inside the cultivation chamber.

Crucially, no definitive interpretation of the LF MF effect can be built upon this single, preliminary result due to the potentially considerable variability introduced by biological and environmental conditions. Consequently, besides the improvement of various technical issues (addressed in subsequent sections), multiple experimental runs must be conducted to rigorously and statistically evaluate any potential biological effect of LF MF.

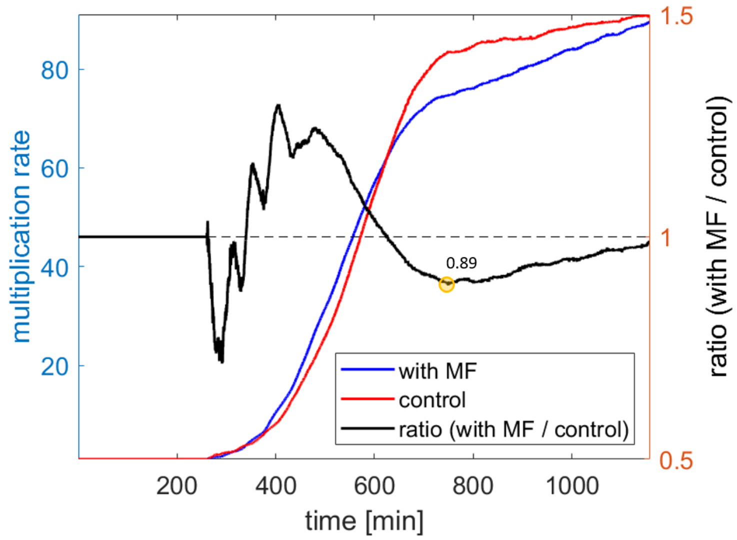

Fig. 7: Cell concentration profile demonstrating LF MF inhibition (3 mT at 800 Hz). The concentration was derived from impedance spectroscopy, calculated using Approach I at the fixed frequency of 3.2 MHz. The primary Y-axis displays the estimated cell multiplication rate for the exposed sample (blue) and the control sample (red). The secondary Y-axis represents the ratio of exposed to control concentrations (black curve). The inhibition rate is quantitatively determined by the minimum value reached by the ratio curve, which occurs at approximately 750 min.

Methodological Challenges

The introduction of the Effect Ratio methodology highlighted several critical areas requiring further specification and corroboration, particularly concerning the two-point calibration process: the first point is biased by early PID stabilization and EIS temperature sensitivity; the second point is biased by slow, linear drift from evaporation and small chamber-to-chamber differences, corrupting the assignment of absolute concentration to impedance traces.

5.2 Challenges in EIS based Cell Concentration Estimation

Mechanical mixing vs. signal stability: Non-magnetic stirring is required for homogeneity, yet mechanical vibrations couple into the impedance readout: higher RPM increased both |Z| and noise. A compromise (lower RPM, vibration isolation, mass loading) is needed to maintain mixing without degrading spectra.

Open systems and evaporation: In open vessels, conductivity and apparent permittivity rise over hours even without cells, mimicking growth. A sealed, stirred bioreactor suppresses evaporation, improves sterility, and stabilizes both conductivity and permittivity after a short transient.

Electrode geometry and probe variability: The cell constant $K=l/A$ ties both resistive and capacitive channels to geometry. Masking electrode area or switching probes (different materials, cell constants, wiring) shifts absolute levels and noise, forcing geometry-specific calibration and limiting cross-probe comparability.

Temperature sensitivity: Permittivity at MHz frequencies changes strongly with temperature; differences of only 0.5 °C can translate into ~10% shifts in the inferred concentration. Tight control and/or explicit thermal compensation are mandatory.

Frequency selection and model choice: Very low frequency adds noise and electrode polarization; very high frequency flattens dynamics. Mid-β-dispersion (≈0.3–4 MHz here) yields the most informative trajectories for single-shell ($\Delta\varepsilon$-type) estimators; impedance-ratio methods may require careful LF/HF pairing and sign handling.

Calibration shortfalls in practice: Discrete addition and dilution series attempts often failed to produce a monotonic, reproducible ε concentration curve especially at low biomass where temperature and ionic micro changes dominate the signal. Even with improved hardware, absolute quantification remained elusive without robust, frequency-specific calibration.

Conductivity permittivity coupling: Time courses of calculated ε and κ were highly correlated (Pearson > 0.98 across 0.3–5 MHz), implying that what appears as a permittivity change is often dominated by medium conductivity shifts driven by metabolism/chemistry rather than membrane polarization alone.

Under these conditions, EIS provides rich, real-time signals but is methodologically fragile for absolute cell concentration: it demands sealed culture, stringent thermal control, vibration mitigation, fixed geometry, careful frequency selection, and validated, probe-specific calibration with awareness that conductivity-driven effects can masquerade as dielectric biomass signatures.

6 Static Cultivation with Turbidimetry-Based Concentration Measurement

After observing limitations with impedance-based monitoring, we adopted a simple, reliable workflow for estimating growth via static cultivation with turbidimetry: no stirring, no impedance probe, sealed vials for sterility, 10 vials total (5 LF MF exposed, 5 control) plus 2 dilution controls (10x) for low-biomass reference. We built a calibration by correlating turbidity (NTU) with Bürker chamber counts from a YPD dilution series, yielding a strong linear fit ($R^2 = 0.972$) and supporting turbidity as a practical estimator of cell concentration in the mid to high density range. At low densities, both methods lose precision: Bürker counts suffer from counting statistics and non-uniform cell distribution, while turbidimetry under-samples scattering events, so results in this regime should be interpreted with caution.

6.1 *Optimal Starting Microbial Concentration*

Optimizing the setup required jointly selecting the initial cell concentration and total cultivation time, which we determined iteratively: practical constraints limited each run to 20 h of cultivation within a 24 h day, so we screened dilutions to keep cells in the desired growth phase over that window. After 20 h at 35 °C, only a 10% inoculum (1:10) reached biomass equivalent to the pre-culture; dilutions beyond ~1:3.2×10^4 yielded ≤50% growth, and at 1:10^7 growth was ≈2.2%. For paired comparisons, we targeted a final biomass window of 20–60% to preserve sensitivity, refined tests across 5×10^4–2×10^5 dilutions and set the working inoculum at a 1.8×10^5-fold dilution (≈306 cells/ml).

6.2 *Modelling of Optimal Duration of Biological Experiment*

To determine the optimal experiment duration, we ran a large, uniform-temperature cultivation (84 vials submerged in a water bath) using the selected inoculum (~306 cells/ml) in two identical thermostatic chambers, tracking turbidity from 12 h across 14 time points (Fig. 8a). We then simulated an LF MF effect as a time shift of the growth curve (delay or advance, Fig. 8b simulates an MF effect as a 2 h delay) and computed absolute and relative differences versus control to find the most discriminative readout time. The analysis showed maximal practical at 18 h, when biomass is ~33% of its eventual maximum (≈1.82×10^7 cells/ml after ~16 doublings).

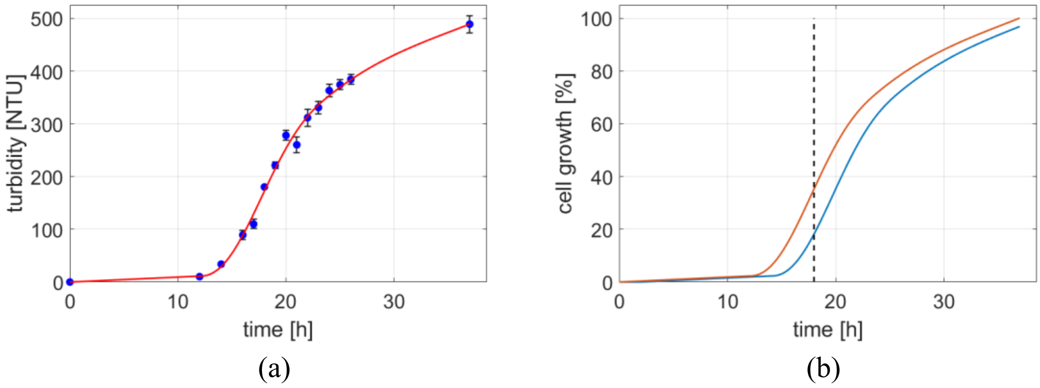

Fig. 8: (a) Growth curve illustrating the increase in cell concentration of Saccharomyces cerevisiae CCY 21-4-99 over time at 35 °C. (b) Simulation of MF impact by delaying growth by 2 hours (blue curve). The vertical line at 18 h indicates the moment of maximum difference between the two growth curves

6.3 *Verifying Pair Experimental Design*

To overcome the common limitations (insufficient temperature control, absence of cross-over/pair designs, and uneven environmental conditions) the experimental platform consists two independently monitored chambers, with cross-over capability, and has real-time temperature tracking in both chambers. Pair experiments (18 h at 35 °C) were run in two modes: both chambers as controls (no MF) and both as tests (50 Hz, 3.5 mT, 4.5 A). Only runs meeting strict thermal criteria were analyzed: each chamber within 35 ± 0.3 °C and the inter-chamber ΔT within ± 0.3 °C.

Results show the two chambers behave equivalently: the mean growth difference between chambers stayed < 1% in control, test, and combined datasets, and a one-sample t-test failed to reject zero mean difference (p = 0.56, 0.78, 0.52). These outcomes confirm the experimental platform's symmetry and reproducibility for pair experiment (Fig. 9).

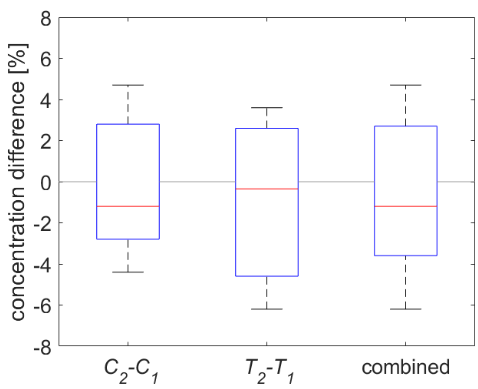

Fig. 9: Boxplots for cell concentration difference between cultivated cultures in two chambers. C-C: both chambers in control mode without MF (N = 5). T-T: both chambers in test mode with MF (N = 5). Combined: merged data from the two previous sets (N = 10).

7 Effect of 50 Hz Magnetic Field on Saccharomyces Cerevisiae Growth

The results presented in this chapter originate from the experimental setup described in chapter 6, which used static cultivation in sealed vials combined with turbidity-based cell concentration measurement.

Data from four types of pair experimental setups were collected for analysis: control–control (C–C), test–test (T–T), test–control (T_1–C_2), and control–test (T_2–C_1), where the subscript denotes the chamber. In total, 58 runs were performed; to ensure reliable comparisons, we retained only runs meeting strict thermal symmetry: both chambers at 35 ± 0.3 °C and inter-chamber ΔT within ± 0.3 °C. This yielded 24 runs for analysis 12 controls (6 C–C, 6 T–T) and 12 tests (6 T_1–C_2, 6 T_2–C_1). The ±0.3 °C threshold balanced platform capability with sample size; broader cutoffs (±0.4/±0.5 °C) produced comparable conclusions.

Outcomes were computed as relative differences in turbidity between chambers for each configuration, and summarized in Fig. 10a. Aggregating per configuration (six independent runs each, five vials per run), Fig. 10b–c contrasts the MF cases against their appropriately ordered control pairs. When MF was applied in chamber 1 (T_1–C_2), the mean growth difference favored the exposed side by ≈ +1.4 %; when MF was applied in chamber 2 (T_2–C_1), the exposed side showed ≈ –2.8 % relative to the reversed controls. These opposing tendencies argue against a consistent MF effect and instead suggest chamber- or run-level variability around zero.

Statistical testing confirmed no significant MF effect. Two-sample comparisons of each MF configuration against its matched control set, as well as a complementary one-sample approach that baseline-corrected each MF dataset by subtracting its corresponding control mean (to account for small non-zero control offsets), all returned p-values between ~0.15 and 0.91. Normality checks guided the use of parametric or nonparametric tests as appropriate; conclusions were unchanged across methods. Because yeast growth is temperature-sensitive, we also applied linear temperature corrections derived from the dataset (narrow and broad ranges); adjusting results by these small slopes did not change statistical outcomes and effect estimates remained non-significant.

In sum, under 50 Hz, 3.5 mT exposure with tight thermal symmetry (35 ± 0.3 °C) and a paired design, the platform shows no measurable impact of LF MF on yeast growth within the precision and detection limits of this study. The small and directionally inconsistent chamber differences observed in Fig. 10 reflect experimental noise rather than a reproducible bioeffect, reinforcing the platform's value for generating clear, well-controlled negative (or positive) findings.

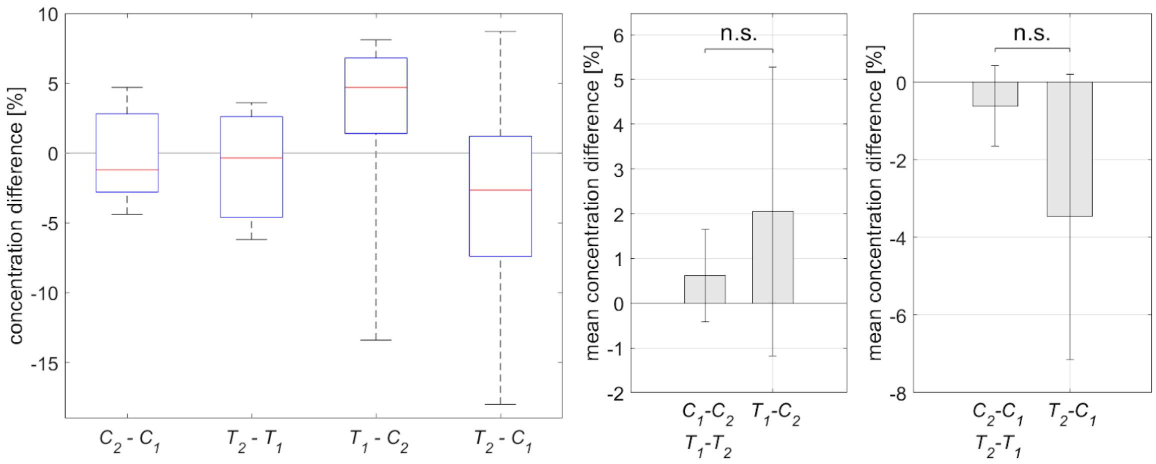

(a) (b) (c)

Fig. 10: (a) Boxplots showing the relative differences in cell concentration between cultures grown in the two cultivation chambers across four different experimental setups ($N = 6$ for each setup). (b) Mean cell concentration difference between chambers in the pair experimental setup for the case of combined control conditions (C_1 - C_2 and T_1 - T_2) and MF applied in chamber 1 (T_1 - C_2). (c) Mean cell concentration difference for the case of combined control conditions (C_2 - C_1 and T_2 - T_1) and MF applied in chamber 2 (T_2 - C_1, $N = 6$). Error bars represent ± SEM

7.1 Discussion

Prior to the LF MF study review (Tab. 1 and Tab. 2), most studies have not documented temperature equality between test and control with the granularity used here. Most reports claimed temperature stability without quantified side-by-side temperature traces or explicit ΔT between groups, leaving room for misattribution of thermal artifacts as field effects. We also found no control–control or test–test checks, nor are any cross-over designs, to confirm that the two chambers behaved equivalently, those procedures, which we considered essential in paired experiments.

In our experiments, brief early overshoot arose after vial insertion: pre-warmed samples still entered slightly below 35 °C, prompting the PID to correct and transiently overshoot. Minimizing this would require reducing the initial sensed drop (≈0.1 °C target) by increasing the thermal mass of the bath relative to sample volume implying a substantially larger reservoir or chamber redesign. Despite this transient, our acceptance criteria (both chambers 35 ± 0.3 °C and inter-chamber $\Delta T \leq \pm 0.3$ °C) ensured thermal symmetry for the analyzed runs.

The static geomagnetic field in the lab was ~56 µT and thus common-mode. Our applied 50 Hz field was 3.5 mT, ~60× larger, so any between-chamber differences reflect the externally driven exposure rather than the background. Under these tightly controlled conditions, we observed no measurable MF effect on yeast growth contrasting with a literature that contains both positive and null reports. Given publication bias toward positive findings and the rarity of rigorous ΔT reporting, we suspect that unnoticed temperature differences (and related design issues) explain a non-trivial share of claimed effects.

Finally, while our exposure exceeded typical residential and office levels by four–five orders of magnitude and still produced no detectable effect, caution is warranted in extrapolating to human safety. Whole organisms possess regulatory and compensatory mechanisms absent in isolated cultures, which could attenuate or under specific conditions, amplify responses. The key contribution here is not only a clear negative result but a validated methodology (paired, temperature-symmetric, cross-over-capable) that future studies can adopt to produce decisive evidence positive or negative on LF MF bioeffects.

8 Conclusions and Main Contributions

The objective of this thesis was to develop a measurement platform for experimentally investigating the effects of weak low-frequency magnetic fields (LF MFs) on living systems, and to establish a rigorous methodological framework for accurate, reproducible assessment of such effects using both established and exploratory cell-concentration readouts.

A state of the art review (Tab. 1 and Tab. 2) mapped biological outcomes against field parameters and design strategies, revealing large variability and frequent gaps in environmental control. Common shortcomings included missing temperature monitoring, no reporting of temperature differences between test and control, absence of validating C/C and T/T pairs, and lack of cross-over designs. Many positive findings could not clearly exclude thermal or positional artifacts, underscoring the need for a new, tightly regulated platform for paired LF MF exposure with high reproducibility criteria that directly informed our system design.

We designed, realized, and tested a comprehensive platform for pairwise LF MF exposure under controlled conditions, integrating:

- Helmholtz coils with verified homogeneity (RSD < 2.6% across 15 points within a 76.5 mm-diameter, 12 mm-high working volume),
- a field-generation chain (waveform generator + high-power amplifier, dual/bridge modes) delivering stable fields up to 5 mT from 10 Hz–2 kHz,
- in-situ temperature regulation with active control. Stability improved from ±1.5 °C (on–off) to ±0.3 °C (PID + optimized heater placement).

Two parallel cultivation chambers enable precise exposed–control comparisons with matched field and temperature, support C/C, T/T, and cross-over runs, and address nearly all methodological weaknesses identified in the review.

We evaluated methods for ex-situ and in-situ growth monitoring. Optical turbidimetry and impedance spectroscopy were selected for their potential to capture dynamic cell-concentration changes and for compatibility with the platform. For impedance, we implemented a fully functional, real-time system (10 Hz–10 MHz, 4-wire) and tested three estimators: (1) permittivity near the β-dispersion characteristic frequency, (2) the capacitance increment ΔC obtained from the imaginary impedance between selected low and high frequencies in the β-dispersion region, and (3) a low/high-frequency impedance ratio.

Despite high-quality instrumentation and tight thermal control, impedance-based estimation was not consistently reliable in this setup. Asami-based curves could appear growth-like, but robust calibration linking impedance metrics to absolute concentration was not achieved; sensor variability, environmental sensitivity, and electrode inconsistencies limited generality. (We note the method's feasibility was demonstrated in a separate study, indicating the approach remains promising with further refinement.) Turbidimetry, in contrast, proved simple, non-invasive, and well-calibrated against Bürker hemocytometer counts, and was adopted as the reference metric.

Using the finalized platform, we conducted paired, temperature-symmetric experiments exposing Saccharomyces cerevisiae to 50 Hz, 3 mT LF MF for 18 h, with replicated runs. Growth was quantified turbidimetrically and analyzed statistically across independent experiments. No statistically significant differences were detected between exposed and control in cell concentration. Within the tested conditions and detection limits, we conclude no significant biological effect of weak LF MF on yeast growth. The platform and methodology provide a reproducible foundation for future, tightly controlled investigations.

In summary, this dissertation delivers substantial technical innovation and methodological rigor crucial for advancing reproducible research in the field of LF MF bioeffects. The key contributions include:

- An established and validated state-of-the-art experimental platform for LF MF exposure, ensuring unprecedented environmental control through tightly controlled thermal symmetry between parallel test and control chambers, minimized coil heating, and quantified magnetic field homogeneity.
- An impedance spectroscopy system for real-time, in-situ cell concentration monitoring was designed, implemented, and subjected to rigorous stress-testing, together with a developed methodology for quantifying LF MF effects.
- A critical assessment of impedance-based cell concentration estimation, clearly identifying key limitations (temperature sensitivity, evaporation, medium conductivity interference, and probe geometry variability).
- Biological effect under strictly controlled pair experimental conditions: 18-hour exposure of Saccharomyces cerevisiae to 50 Hz, 3 mT demonstrated no statistically significant difference in cell growth.

This dissertation fundamentally raises the standard for experimental methodology in the field of LF MF bioeffects. Although no reliable evidence of significant biological effects was definitively isolated, the primary contribution lies in the robust, reproducible platform and rigorous protocols developed, which provide the scientific community with an essential foundation for clear and unambiguous investigation. In the long term, this work may pave the way for defining exposure guidelines or enabling novel applications in MF-based biotechnology, including the development of diagnostic and therapeutic technologies reliant on electromagnetic inhibition or stimulation.

Author's Publications

Publications in scientific journals:

Vu Viet H., Kremnicky L., Bereta M., Teplan M. (2025). Experimental Platform for Investigation of Low-Frequency Magnetic Field Effects on Cells. *Measurement Science Review*, 25 (2), 83-92. http://doi.org/10.2478/msr-2025-0011

Bereta M., Teplan M., Zakar, T., **Vu Viet H.**, Cifra M., Chafai D.E. (2024). Biological Autoluminescence Enables Effective Monitoring of Yeast Cell Electroporation. *Biotechnology Journal*, 19 (4), 2300475, https://doi.org/10.1002/biot.202300475

Publications in conference proceedings:

Teplan, M., **Vu Viet, H.**, Kremnicky, L., Bereta, M. (2025). Growth of Saccharomyces Cerevisiae in a 50 Hz Magnetic Field. *MEASUREMENT 2025*: *Proceeding of the 15th International Conference on Measurement*, 19-22, ISBN 978-80-69159-01-3, https://doi.org/10.23919/MEASUREMENT66999.2025.11078695

Vu Viet H., Teplan M., Kremnicky L., Bereta M. (2025). Optimization of Physical and Biological Parameters for Studying Microorganism Responses to Low-Frequency Magnetic Fields. *MEASUREMENT 2025*: *Proceeding of the 15th International Conference on Measurement*, 245-248, ISBN 978-80-69159-01-3, https://doi.org/10.23919/MEASUREMENT66999.2025.11078721

Vu Viet, H., Teplan, M. (2023). Development of An Experimental Platform for The Measurement of Biological Response of Low-Frequency Magnetic Fields. *MEASUREMENT 2023*: *Proceeding of the 14th International Conference on Measurement*, 113-116, ISBN 978-80-972629-7-6, https://doi.org/10.23919/MEASUREMENT59122.2023.10164326

Bereta, M., Teplan, M., Chafai D.E., Zakar T., **Vu Viet H.**, Cifra M. (2023). Assessment of Yeast Cells Electroporation by Autoluminescence and Impedance Measurements. *MEASUREMENT 2023*: *Proceeding of the 14th International Conference on Measurement*, 109-112, ISBN 978-80-972629-7-6, https://doi.org/10.23919/MEASUREMENT59122.2023.10164612

Vu Viet H., Teplan M. (2021). Impact of Magnetic Field on Yeast Cells Monitored by Impedance Spectroscopy. *IWIS 2021: Proceeding of International Workshop on Impedance Spectroscopy*, 85-88, ISBN 978-1-6654-9472-4, https://doi.org/10.1109/IWIS54661.2021.9711789

Teplan M., **Vu Viet H.**, Bereta M., Bajla I. (2021). Measurement System for Monitoring of Magnetic Field Effects on Yeast Cells by Impedance Spectroscopy. *MEASUREMENT 2021: Proceeding of the 13th International Conference on Measurement*, 198-201, ISBN 978-80-972629-5-2, http://doi.org/10.23919/Measurement52780.2021.9446776

Abstracts in scientific conferences:

Bereta M., Teplan M., Zakar, T., **Vu Viet H.**, Cifra M., Chafai D.E. (2025). Biological Autoluminescence as a Real-Time Monitoring Tool for Yeast Electroporation, BioEM2025, *Book of Abstracts*, International conference on bioelectromagnetics, Rennes, France, OS04-02.

Vu Viet H., Teplan M. (2023). Development of An Experimental Platform for the Measurement of Low-Frequency Magnetic Field Effect on Yeast Cells. *ZBORNÍK ABSTRAKTOV: XLIV. DNÍ LEKÁRSKEJ BIOFYZIKY*, 44th Conference Day of Medical Biophysics, Stara Lesna, Slovakia, 84-85 https://www.44dlb.sk/pre_autorov/zbornik-abstraktov/

Teplan M., **Vu Viet H**. (2021), Impedance Spectroscopy Monitoring of Magnetic Field Effects on Yeast Cells. *Abstract Book International Workshop on Impedance Spectroscopy*, 14th International Workshop on Impedance Spectroscopy, Chemnitz, Germany, 151-154, ISBN 978-3-949744-00-6

Participation in congresses and conferences:

14th International Conference on Measurement, May 29th – May 31st, 2023, Institute of Measurement Science SAS, Smolenice Castle, Smolenice, Slovakia

44th Conference Day of Medical Biophysics, May 31st – June 2nd, 2023, Faculty of Medicine Comenius University Bratislava, Congress center of SAS academia, Stara Lesna, Slovakia

14th International Workshop on Impedance Spectroscopy, September 29th – October 1st, 2021, Technische Universität Chemnitz, Chemnitz, Germany

13th International Conference on Measurement, May 17th – May 19th, 2021, Institute of Measurement Science SAS, Bratislava, Slovakia

References

[1] Vistnes A.I., Ramberg G.B., Bjørnevik L.R., Tynes T., Haldorsen T. (1997). Exposure of children to residential magnetic fields in Norway: is proximity to power lines an adequate predictor of exposure? *Bioelectromagnetics*, 18(1), 47-57. PMID: 9125232.

[2] Floderus B., Stenlund C., Persson T. (1999). Occupational Magnetic Field Exposure and Site-Specific Cancer Incidence: A Swedish Cohort Study. *Cancer Causes & Control*, 10(5), 323–332. http://www.jstor.org/stable/3553683

[3] National Radiological Protection Board (2001). ELF Electromagnetic Fields and the Risk of Cancer: Report of an Advisory Group on Non-Ionising Radiation. Document of NRPB, 12(1), 1–179, Chilton, UK.

[4] ICNIRP (2010). Guidelines for limiting exposure to time-varying electric and magnetic fields (1 Hz–100 kHz). *Health Physics*, 99(6), 818–836. https://doi.org/10.1097/HP.0b013e3181f06c86

[5] BfS (2023). Limit values in Europe for electromagnetic fields. Federal Office for Radiation Protection (Bundesamt für Strahlenschutz), Germany. Available at: https://www.bfs.de/EN/topics/emf/expansion-grid/protection/limit-values-europes/limit-values-europe.html

[6] Tota M., Jonderko L., Witek J., Novickij V., Kulbacka, J. (2024). Cellular and molecular effects of magnetic fields. *International Journal of Molecular Sciences*, 25 (16), 8973. https://doi.org/10.3390/ijms25168973

[7] Lee H. C., Hong M.-N., Jung S. H., Kim B. C., Suh Y. J., Ko Y.-G., Lee Y.-S., Lee B.-Y., Cho Y.-G., Myung S.-H., Lee J.-S. (2015). Effect of extremely low frequency magnetic fields on cell proliferation and gene expression. *Bioelectromagnetics*, 36 (7), 506-516. https://doi.org/10.1002/bem.21932

[8] Zhang M., Li X., Bai L., Uchida K., Bai W., Wu B., Xu W., Zhu H., Huang H. (2013). Effects of low frequency electromagnetic field on proliferation of human epidermal stem cells: An in vitro study. *Bioelectromagnetics*, 34 (1), 74-80. https://doi.org/10.1002/bem.21747

[9] Pasi F., Sanna S., Paolini A., Alquati M., Lascialfari A., Corti M. E., Di Liberto R., Cialdai F., Monici, M., Nano R. (2016). Effects of extremely low-frequency magnetotherapy on proliferation of human dermal fibroblasts. *Electromagnetic Biology and Medicine*, 35 (4), 343-352. https://doi.org/10.3109/15368378.2016.1138123

[10] Radil R., Carnecka L., Judakova Z., Pobocikova I., Bajtos M., Janousek L. (2024). Exploring non-thermal mechanisms of biological reactions to extremely low-frequency magnetic field exposure. *Applied Sciences*, 14 (20), 9409. https://doi.org/10.3390/app14209409

[11] Tang R., Xu Y., Ma F., Ren J., Shen S., Du Y., Hou Y., Wang T., (2016). Extremely low frequency magnetic fields regulate differentiation of regulatory T cells: Potential role for ROS-mediated inhibition on AKT, *BioElectroMagnetics*, 37 (2), 89-98. https://doi.org/10.1002/bem.21954

[12] Lai H. (2021). Genetic effects of non-ionizing electromagnetic fields. *Electromagnetic Biology and Medicine*, 40 (2), 264-273. https://doi.org/10.1080/15368378.2021.1881866

[13] Duong C. N., Kim J. Y. (2016). Exposure to electromagnetic field attenuates oxygen-glucose deprivation-induced microglial cell death by reducing intracellular Ca2+ and ROS. *International Journal of Radiation Biology*, 92 (4), 195-201. https://doi.org/10.3109/09553002.2016.1136851

[14] Wertheimer N., Leeper, E. (1979). Electrical Wiring Configurations and Childhood Cancer, *American Journal of Epidemiology*, 109 (3), 273-284. https://doi.org/10.1093/oxfordjournals.aje.a112681

[15] Turner M. C., Benke G., Bowman J. D., Figuerola J., Fleming S., Hours M., Kincl L., Krewski D., McLean D., Parent M. E., Richardson L., Sadetzki S., Schlaefer K., Schlehofer B., Schüz J., Siemiatycki J., van Tongeren M., Cardis E. (2014). Occupational Exposure to Extremely Low-Frequency Magnetic Fields and Brain Tumor Risks in the INTEROCC Study, *Cancer Epidemiology Biomarkers and Prevention*, 23 (9), 1863-1872. https://doi.org/10.1158/1055-9965.epi-14-0102

[16] Savitz D. A., Liao D., Sastre A., Kleckner R.C., Kavet R. (1999) Magnetic Field Exposure and Cardiovascular Disease Mortality among Electric Utility Workers, *American Journal of Epidemiology*, 149 (2), 135-142. https://doi.org/10.1093/oxfordjournals.aje.a009779

[17] Caliogna L., Medetti M., Bina V., Brancato A. M., Castelli A., Jannelli E., Ivone A., Gastaldi G., Annunziata S., Mosconi M., Pasta G. (2021). Pulsed electromagnetic fields in bone healing: Molecular pathways and clinical applications. *International Journal of Molecular Sciences*, 22 (14), 7403. https://doi.org/10.3390/ijms22147403

[18] Gualdi G., Costantini E., Reale M., Amerio, P. (2021). Wound repair and extremely low frequency-electromagnetic field: Insight from in vitro study and potential clinical application. *International Journal of Molecular Sciences*, 22 (9), 5037. https://doi.org/10.3390/ijms22095037

[19] Xu A., Wang Q., Lin, T. (2020). Low-frequency magnetic fields (LF MFs) inhibit proliferation by triggering apoptosis and altering cell cycle distribution in breast cancer cells. *International Journal of Molecular Sciences*, 21 (8), 2952. https://doi.org/10.3390/ijms21082952

[20] Wang S., Zhou X., Huang B., Wang Z., Zhou L., Wang M., Yu L., Jiang H. (2016). Noninvasive low-frequency electromagnetic stimulation of the left stellate ganglion reduces myocardial infarction-induced ventricular arrhythmia. *Scientific Reports*, 6 (1), 30783. https://doi.org/10.1038/srep30783

[21] Rick O., von Hehn U., Mikus E., Dertinger H., Geiger, G. (2017). Magnetic field therapy in patients with cytostatics-induced polyneuropathy: A prospective randomized placebo-controlled phase-III study. *Bioelectromagnetics*, 38 (2), 85-94. https://doi.org/10.1002/bem.22005

[22] Sincak M., Luptakova A., Matusikova I., Jandacka P., Sedlakova-Kadukova, J. (2023). Application of a magnetic field to enhance the environmental sustainability and efficiency of microbial and plant biotechnological processes. *Sustainability*, 15 (19), 14459. https://doi.org/10.3390/su151914459

[23] Liu J., Wang D., Wang H., Yang N., Hou J., Lv X., Gong L. (2024). Low frequency magnetic field assisted production of acidic protease by Aspergillus niger. *Archives of Microbiology*, 206, 273. https://doi.org/10.1007/s00203-024-04004-5

[24] Novák J., Strašák, L., Fojt, L., Slaninová, I., Vetterl, V. (2007). Effects of low-frequency magnetic fields on the viability of yeast Saccharomyces cerevisiae. *Bioelectrochemistry*, 70 (1), 115-121. https://doi.org/10.1016/j.bioelechem.2006.03.029

[25] Adey W.R. (1980). Frequency and power windowing in tissue interactions with weak electromagnetic fields. *Proceedings of IEEE*, 68 (1), 119–125. https://doi.org/10.1109/PROC.1980.11591

[26] Liboff A. R., (1985). Geomagnetic cyclotron resonance in living cells. *Journal of Biological Physics*, 13, 99-102. https://doi.org/10.1007/BF01878387

[27] Lednev V. V. (1991). Possible mechanism for the influence of weak magnetic fields on biological systems. *BioElectroMagnetics*, 12 (2), 71-75. https://doi.org/10.1002/bem.2250120202

[28] Belova N. A., Panchyeluga, V. A. (2010). Lednev's model: Theory and experiment. *Biophysics*, 55 (4), 661-674. https://doi.org/10.1134/S0006350910040263

[29] Steiner U. E. and Ulrich T. (1989). Magnetic field effects in chemical kinetics and related phenomena, *Chemical Reviews*, 89 (1), 51-147. https://doi.org/10.1021/cr00091a003

[30] Woodward J. R. (2002). Radical Pairs in Solution, *Progress in Reaction Kinetics and Mechanism*, 27 (3), 165-207. https://doi.org/10.3184/007967402103165388

[31] Barnes F. S. and Greenebaum, B. (2015). The effects of weak magnetic fields on radical pairs, *BioElectroMagnetics*, 36 (1), 45-54. https://doi.org/10.1002/bem.21883

[32] Rochev Y. A., Narimanov A. A., Sosunov E. A., Kozlov A. N., Lednev V. V. (1990). Effects of Weak Magnetic-field on the Rate of Cell-Proliferation in Culture. *Studia Biophysica*, 135 (1-2), 93-98.

[33] Yost M. G., Liburdy, R. P. (1992). Time-varying and static magnetic fields act in combination to alter calcium signal transduction in the lymphocyte, *FEBS Letters*, 296 (2), 117-122. https://doi.org/10.1016/0014-5793(92)80361-j

[34] Bodewein L., Schmiedchen K., Dechent D., Stunder D., Graefrath D., Winter L., Kraus T., Driessen S. (2019). Systematic review on the biological effects of electric, magnetic and electromagnetic fields in the intermediate frequency range (300 Hz to 1 MHz). *Environmental Research*, 171, 247-259. https://doi.org/10.1016/j.envres.2019.01.015

[35] Buchachenko A. (2016). Why magnetic and electromagnetic effects in biology are irreproducible and contradictory? *Bioelectromagnetics*, 37 (1), 1-13. https://doi.org/10.1002/bem.21947

[36] International Commission on Non-Ionizing Radiation Protection (ICNIRP). (2025). Gaps in knowledge relevant to the "ICNIRP guidelines for limiting exposure to time-varying electric, magnetic and electromagnetic fields (100 kHz TO 300 GHz)". *Health Physics*, 182 (2), 190-202. https://doi.org/10.1097/HP.0000000000001944

[37] Makinistian, L., Vives, L. (2025). Devices, facilities, and shielding for biological experiments with static and extremely low frequency magnetic fields. *IEEE Journal of Electromagnetics, RF and Microwaves in Medicine and Biology*, 9 (2), 141-156. https://doi.org/10.1109/JERM.2024.3419232

[38] Ronniger M., Aguida B., Stacke C., Chen Y., Ehnert S., Erdmann N., Eschenburg G., Falldorf K., Pooam M., Wing A., Ahmad M. (2022). A novel method to achieve precision and reproducibility in exposure parameters for low-frequency pulsed magnetic fields in human cell cultures. *Bioengineering*, 9 (10), 595. https://doi.org/10.3390/bioengineering9100595

[39] Song K., Im S. H., Yoon Y. J., Kim H. M., Lee H. J., Park G. S. (2018). A 60 Hz uniform electromagnetic field promotes human cell proliferation by decreasing intracellular reactive oxygen species levels. *PLoS One*, 13 (7), e0199753. https://doi.org/10.1371/journal.pone.0199753

[40] Tian H., Zhu, H., Gao C., Shi M., Yang D., Jin M., Wang F., Sui X. (2023). System-level biological effects of extremely low-frequency electromagnetic fields: An in vivo experimental review. *Frontiers in Neuroscience*, 17, 1247021. https://doi.org/10.3389/fnins.2023.1247021

[41] Ye H., Cotic M., Carlen P.L. (2007). Transmembrane potential induced in a spherical cell model under low-frequency magnetic stimulation. *J Neural Eng.*, 4(3):283-93. https://doi.org/10.1088/1741-2560/4/3/014.

[42] Cecchetto C., Maschietto M., Boccaccio P., Vassanelli S. (2015). Enhancement of Kv1.3 Potassium Conductance by Extremely Low Frequency Electromagnetic Field. *Bioelectromagnetics*, https://doi.org/10.48550/arXiv.1508.06135

[43] Rishabh R., Zadeh-Haghighi H., Salahub D., Simon C. (2022). Radical pairs may explain reactive oxygen species-mediated effects of hypomagnetic field on neurogenesis. *PLoS Comput Biol*, 18(6). https://doi.org/10.1371/journal.pcbi.1010198

[44] Wang H., Zhang X. (2017). Magnetic Fields and Reactive Oxygen Species. *Int J Mol Sci.*, 18(10). https://doi.org/10.3390/ijms18102175

[45] Cifra M, Fields J.Z., Farhadi A. (2011). Electromagnetic cellular interactions. *Progress in Biophysics Molecular Biology*, 105(3), 223-246. https://doi.org/10.1016/j.pbiomolbio.2010.07.003

[46] Radil R., Barabas J., Janousek L., Bereta, M. (2020). Frequency-dependent alterations of S. Cerevisiae proliferation due to LF EMF exposure. *Advances in Electrical and Electronic Engineering*, 18(2), 99-103. https://doi.org/10.15598/aeee.v18i2.3461

[47] An G.-Z., Xu, H., Zhou Y., Du L., Miao X., Jiang D.-P., Li K.-C., Guo G.-Z., Zhang, C., Ding, G.-R. (2015). Effects of long-term 50Hz power-line frequency electromagnetic field on cell behavior in Balb/c 3T3 cells. *PLoS One*, 10 (2), e0117672. https://doi.org/10.1371/journal.pone.0117672

[48] Asami K., Yonezawa T. (1995). Dielectric analysis of yeast cell growth, *Biochimica et Biophysica Acta*, 1245, 99-105. https://doi.org/10.1016/0304-4165(95)00074-L

[49] Yardley J.E., Douglas B.K., Barrett J., Davey C.L. (2000). On-Line, Real-Time Measurements of Cellular Biomass using Dielectric Spectroscopy, *Biotechnology and Genetic Engineering Reviews*, 17(1), 3-36, https://doi.org/10.1080/02648725.2000.10647986

[50] Soley A., Lecina M., Gámez X., Cairó J.J., Riu P., Rosell X., Bragós R., Gòdia F. (2005). On-line monitoring of yeast cell growth by impedance spectroscopy. *J Biotechnol,* 118(4), 398-405. https://doi.org/10.1016/j.jbiotec.2005.05.022

[51] Foster K. R., Schwan H. P. (1989). Dielectric Properties of Tissues and Biological Materials: A Critical Review, *Critical Reviews in Biomedical Engineering*, 17 (1), 25-104. PMID: 2651001

[52] Bragos R., (1997) Contribution to the characterization of biological systems using electrical impedance spectroscopy. Ph.D. Dissertation. Polithecnic University of Catalonia, Barcelona